Controlled Cavity Collapse: Scaling laws of Drop Formation

A. Said Ismail[a], Alfonso M. Gañán-Calvo[b], J. Rafael Castrejón-Pita[c], Miguel A. Herrada[b] and Alfonso. A. Castrejón-Pita[a,‡]

The formation of transient cavities at liquid interfaces occurs in an immense variety of natural processes, among which the bursting of surface bubbles and the impact of a drop on a liquid pool are salient. The collapse of a surface liquid cavity is a well documented natural process that leads to the ejection of a thin and fast jet. Droplets generated through this process can be one order of magnitude smaller than the cavity's aperture, and are consequently of interest in drop on demand inkjet applications. In this work, the controlled formation and collapse of a liquid cavity is analyzed, and the conditions to minimize the resulting size and number of ejected drops are determined. The experimental and numerical models are simple and consist of a liquid reservoir, a nozzle plate with the discharge orifice, and a moving piston actuated by single half-sine-shaped pull-mode pulses. The size of the jetted droplet is described by a physical model resulting in a scaling law that is numerically and experimentally validated.

1 Introduction

The controllable generation of small droplets and aerosols is of great importance in a large variety of technologies, ranging from drug delivery, microfluidics, crop spraying and inkjet printing. In particular, inkjet has been a key driver in the recent interest on droplet generation techniques as it is directly relevant to a variety of modern digital non-contact manufacturing processes, such as graphic printing[1], fabrication of transistors[2], biochip arraying[3], bioprinting[4] and 3D printing[5,6]. Drop on Demand generators (DoD) are attracting interest due to their ability to controllably deliver minuscule volumes of materials onto a variety of surfaces in a digital non-contact process[7–10].

DoD technologies based on piezoelectric elements were initially proposed by Zoltan[11] in 1972, and later improved to its most common configuration by Kyser and Sears[12] in 1976. The simplest design consists of a glass capillary bonded to a piezoelectric element, with a small nozzle at one of its ends[13]. By carefully selecting a suitable voltage pulse, the capillary is squeezed and/or relaxed, and a droplet similar in size to that of the nozzle is ejected. The overarching challenge faced by the piezo-DoD method is finding the appropriate shape, amplitude and duration of the voltage pulse (the so-called 'waveform' in the inkjet jargon) which will actuate the piezo-element and ultimately produce one droplet per pulse. Great care is taken (with fine tuning carried out empirically by trial-and-error methods) to produce one single droplet without the generation of the undesirable so-called satellite droplets.

The ability to control the droplet volume is of fundamental importance, specially if one desires to define or increase printing resolution while also reducing fluid consumption. In particular, minimizing the droplet size in a controllable fashion has therefore become a major driver, and challenge, for the scientific community. One immediate solution is to reduce the nozzle size[14–19]. However, this leads to many problems as smaller nozzles are prone to clogging and are difficult to manufacture, clean and maintain. Methods to reduce the droplet size without necessarily reducing the size of the nozzle have then become desirable. Chen and Basaran[20,21] in 2001 developed a new technique to produce droplets that are 50% smaller than the nozzle radius by controlling and exploiting the capillary, viscous and inertial time scales in a piezo-driven squeeze-mode glass nozzle. This was achieved by replacing the traditional pull-push pulse by a pull-push-pull waveform to suppress the formation of a primary 'large' droplet while simultaneously inducing the detachment of a *tongue* of fluid which led to the formation of a tiny droplet, smaller than the diameter of the nozzle. A few years later, the same group devised another method[22], for the ejection of even smaller droplets from such nozzles. The method works by finding and exploiting resonances between capillary waves at the surface of the meniscus and an oscillatory inflow, driven by consecutive sinusoidal waveforms. The hydrodynamic interaction between these surface capillary waves and oscillatory inflows led to the generation of a short-lived high-pressure region in the centre of the capillary just under the surface of the interface/meniscus. If these pres-

[a] *Department of Engineering Science, University of Oxford, Oxford OX1 3PJ, UK*
[b] *Dept. Ing. Aerospacial y Fluidomecánica, Universidad de Sevilla, Camino de los Descubrimientos s/n 41092, Spain*
[c] *School of Engineering and Materials Science, Queen Mary, University of London, E1 4NS, UK*
‡ Tel: +44 (0)1865 277921; E-mail:alfonso.castrejon-pita@eng.ox.ac.uk

sures were high-enough to overcome surface tension, *ultra-small* droplets were ejected from the center of the meniscus. In a different work[23], a modulation of the size of the ejected droplets in a DoD printhead was achieved by stimulating multiple piezoelectric elements with different spectral distributions, each exciting a different resonance modes at the fluid interface. By tailoring waveforms this way, they where capable of stimulating the fluid interface to oscillate with one single mode while at the same time quenching others. If the amplitude of the perturbation and hence the oscillation was large enough, a droplet, with a size comparable to that of the center excursion of the oscillating meniscus, was ejected. Since the size of such zone for high-order oscillation modes were much smaller than the orifice, the generated inkjet droplets were significantly smaller than the nozzle.

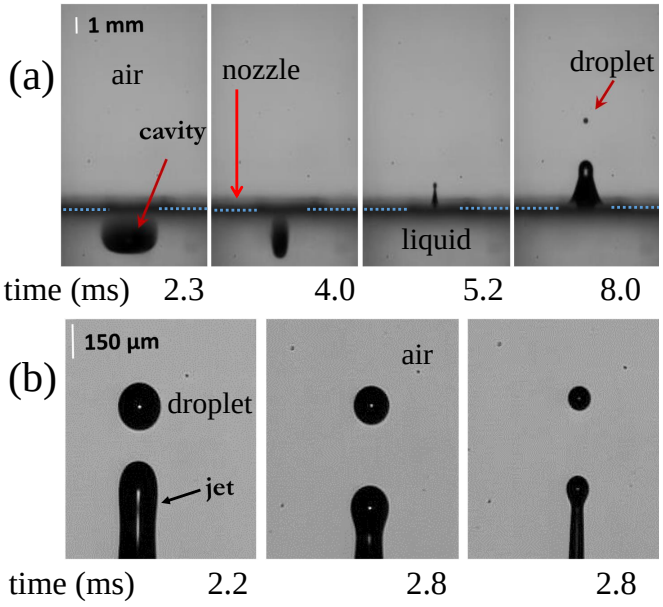

Fig. 1 a) Single droplet ejection from a controlled cavity collapse using Silicone oil (10 cSt) and a 2 mm (diameter) nozzle. b) Zoom into the pinch-off region, showing the change in the size of the ejected droplet for three different piston speeds at approximately the same time. All the images were obtained using a shadowgraphy system, in which drastic changes in refractive indices result high intensity contrasts. Therefore, both the cavity and droplet appear as dark regions. In this case, without losing generality or applicability of the system, the system was arranged in such a way that the droplets are traveling upwards.

On the other hand, researchers have been reported the generation of thin and fast jets after the collapse of liquid surface cavities. This phenomenon is a common source of fine aerosols of mechanical origin from quasi-static liquid surfaces, examples of these are bubbling[24–27] and droplet or solid impact[28] onto liquid pools. In most of these examples, a drop, or series of drops are generated as the result of the cavity collapse, rasing the potential of using such a violent event to produce drops on demand. Based on the phenomenon of cavity collapse, Castrejón-Pita *et al.*[29] devised an alternative design to produce diminutive droplets by carefully controlling the pressure inside a simple liquid-filled reservoir in order to induce the formation and sudden collapse of a small liquid cavity at the interface of an open orifice - the nozzle. Central to the performance of this system is the application of a negative pressure pulse which creates a cavity at the nozzle (inverted meniscus) followed by its subsequent rapid collapse, leading to the formation of a thin and fast jet, as shown in Fig. 1. Under the right conditions, a single, small and fast droplet breaks up from the jet's tip, with the rest of the ejected liquid recoiling back into the reservoir. A major advantage of this system is its clogging-proof nature, as it can handle heavily loaded liquids (e.g. pigment-based inks and colloids) while still being able to produce very small droplets. Also, depending on the actuation and timescales of the piston, this system produces a wider droplet-size spectrum compared to conventional methods. In this sense, this system is analogous to the flow focusing method[30] for steady jet emission. In this work, we present scaling arguments to predict droplet generation from the collapse of liquid cavities. Compared to the problem of jet ejection from bubble bursting[25,36–39], the number of degrees of freedom and operating parameters makes this problem much more complex, but yet we show its main features are similar to the much simpler former natural process. In this regard, we show that the new degrees of freedom bring out their associated non-dimensional parameters without compromising the basic physical principles shared with bubble bursting, but adding new possibilities of fine-tuning for various practical applications. The approach is also practical as it aims to control the size of droplets making the system useful in inkjet applications[7,9].

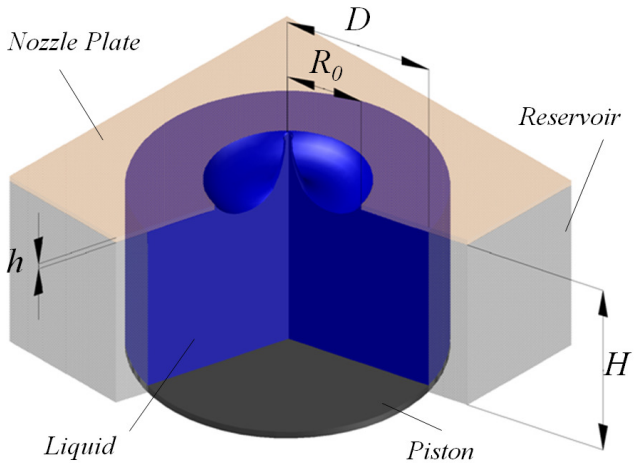

Fig. 2 Sketch of the droplet generator system highlighting the main dimensions (not in scale).

2 Experimental setup

The systematic parametric study carried out for this investigation included both experiments and numerical simulations. We used a setup based on[29] to jet liquid droplets from collapsing cavities. The schematic view of the experimental setup is shown in both Figs. 2 and 3.

In brief, the experiment comprises a reservoir with an internal shape of that of a circular cylinder, machined out of poly-

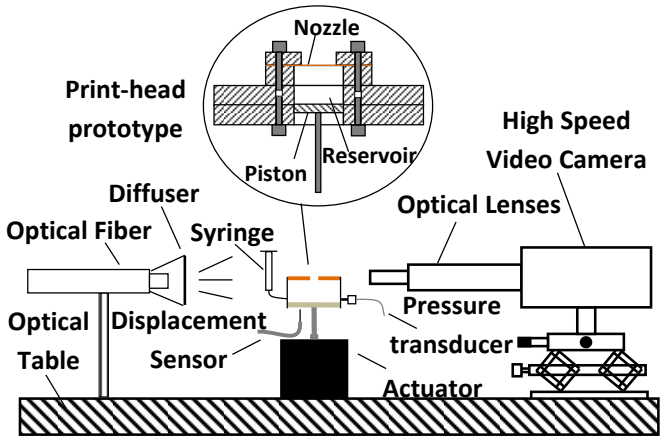

Fig. 3 Experimental setup comprising the droplet generator and the imaging system assembled on a vibration-reduction optical table.

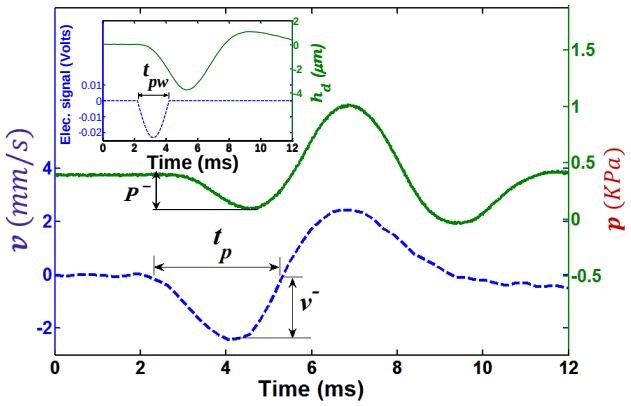

Fig. 4 Driving Electrical waveform pulse and its corresponding piston displacement h_d (top left figure), piston velocity v and the pressure inside the reservoir p (main figure). t_{pw} and t_p are the pulse widths in terms of electrical signal and velocity respectively. Our results show that the driving pulse width and the time for cavity collapse occur at the same order of magnitude, typically few milliseconds. Dataset available in supplemental material[40].

methyl methacrylate, with a diameter $D = 30.0$ mm and height of $H = 20.0$ mm. Similar to the original design in[29] a thin brass sheet of thickness $h = 0.25$ mm with a circular nozzle with radius $R_0 = 1$ mm in its center is fixed to the top of this reservoir, Fig. 2. The bottom end consists of a circular piston which moves by the action of an elecro-mechanical actuator (YMC MS-20), which is in turn driven by a simple pull-mode (half-cycle) sine waveform. The input signal for the piston which produces the cavity is plotted in Fig. 4. The properties of the sine-shaped pulse, such as amplitude and width, are designed within a LabView code. The waveform is therefore generated by a National Instrument acquisition card (USB X Series) and amplified by an integrated amplifier (ROTEL RA-921). A fibre optic displacement sensor (D6-C1H1) and a pressure transducer (Honeywell 40PC001B) are utilized to measure the displacement of the piston and the pressure inside the reservoir, respectively. When the negative pulse is applied, and since the fluid is pinned to the circular nozzle, the meniscus is pulled back into the reservoir forming a liquid cavity. Then, the piston moves towards the nozzle, producing the positive pressure that drives the collapse of the cavity subsequently ejecting a thin liquid jet. Finally, the tip of the jet breaks up, delivering a fast droplet with a size comparable to that of the jet. After breakup, the meniscus relaxes to its original position at the nozzle. For the experiments described in the following text, the input pulse width is set to $t_{pw} = 4.2$ ms.

Images were typically captured at $50,000$ frames per second by a high speed camera (Phantom V12.1) coupled to a macro lens (90mm Tamron) or a microscope lens (12x Navitar lens). A cool-white light source (PhotoFluor II) coupled to a micro-structured optical diffuser (Thorlabs) provided uniform lighting to back-illuminate the system. The camera field of view was of 5.1×8.0 mm^2 in which the pixel size is equal to $0.24\,\mu$m. The cavity collapse, the jetting and the droplet position were recorded by high-speed imaging at all times during the jetting process. The diameter of the droplet was obtained by an image analysis software (ImageJ) after calibration. The working fluid was introduced into the reservoir through a tube connected to a syringe opened to the atmosphere. The syringe is mounted on a micrometre stage to fill and level off the reservoir and to control the interface formed at the orifice (the meniscus).

3 Numerical simulations

Numerical simulations were based on mass continuity, momentum conservation, and liquid volume fraction equations for the incompressible flow regime and were resolved by the VoF scheme, implemented in the commercial solver FLUENT14.0. The axisymmetric configuration of the numerical simulations is illustrated in Fig. 5(a). An uniform velocity distribution at the inlet was assumed, which corresponded to the velocity of the piston $v(t)$. Additionally, a uniform pressure distribution was prescribed over the outlet section, which was located $H/2$ away from the nozzle. The initial conditions for the pressure and velocity fields are considered to be zero in both the liquid and gas phases. Finally, nonslip boundary conditions were imposed at the solid walls. A mesh consisting of 286 792 rectangular cells was used to spatially discretise the equations. In these simulations, two mesh sizes (5 and 500 μm per mesh length unit) were used to speed up the computational time, i.e. a finer mesh was used in the area covered by the movement of the meniscus/cavity. In our experiments and simulations, our droplet diameter ranged between 58 and 800 μm. Hence, the mesh size is about 12 times smaller than the smallest droplet which is enough to avoid numerical diffusion at the droplet interface. Fig. 5(b) shows the mesh distribution; in green the fine mesh and in light-blue the coarse mesh. Our stability analysis show that our results are not affected by this mesh selection. The interface between the two phases was tracked by solving the continuity equation for the volume fraction of the liquid phase. This calculation was performed by using an explicit time-marching scheme, while the rest of the equations were solved implicitly. The time step Δt was around 0.5 μs to ensure that the global Courant number $Co = v_m \Delta t / \Delta y$ (where v_m is the mean velocity in the cell and Δy is the cell size) was less than unity.

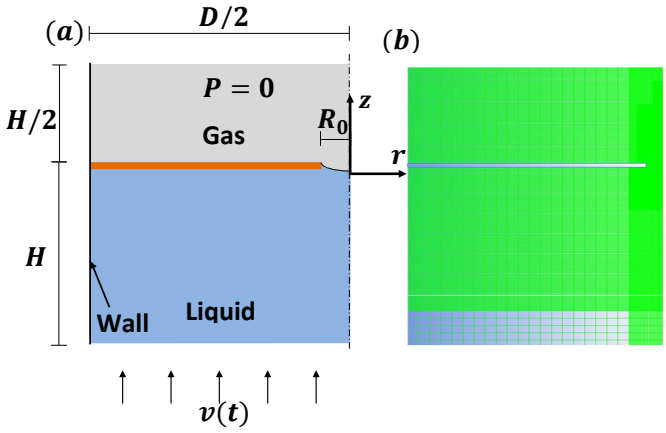

Fig. 5 (a) Simulation domain and (b) numerical mesh; in green the fine mesh and in light-blue the coarse mesh.

For the spatial discretisation of the equations, the third-order modified MUSCL scheme[41] was used to obtain the face fluxes whenever a cell was completely immersed in a single phase. When the cell was near the interface, the GEO-RECONSTRUCTION algorithm was applied. The pressure corrections were computed with the bodyforce-weighted scheme, and the pressure-velocity coupling was treated with the PISO method[42] in a segregated solver. All the simulations were conducted with $D = 30$ mm and $H = 20$ mm.

Further considerations

In order to compare numerical and experimental results a number of practical considerations were required. First, the reservoir in the numerical model contains only one aperture, i.e. the nozzle. In contrast, the experimental setup has the additional liquid inlet used to adjust the position of the meniscus. Secondly, in the numerics the nozzle plate was modelled as a solid rigid body but the thin brass plate on the prototype could suffer small deformations under the applied pressure. Consequently, during the pull phase in the experiment, the cavity volume (V_{cavity}) is equal to the displaced liquid volume by the action of the piston (V_{piston}) minus the volume displaced inside the syringe and the volume displaced by the plate deformation (see the difference in Fig. 6. In order to take these effects into account the velocity of the piston was adjusted to produce the same cavity volume as in the experiment at the peak backward piston displacement. V_{cavity} was measured by extracting the volume of cavity using image analysis. V_{piston} was in turn calculated by multiplying the displacement of the piston by the area of the reservoir. Within the studied experimental range, a cavity to piston displacement volume ratio of $V_{cavity}/V_{piston} \simeq 0.67$ was determined. Simulations neither include the plate deformation nor the feeding system. Consequently, the piston velocity amplitude v^-, in terms of the piston displacement h_p, is calculated to give the same cavity volume as in the experiment:

$$0.67 V_{piston} = A \int v^- dt, \tag{1}$$

$$v^- = 0.67 \frac{dh_p}{dt}, \tag{2}$$

where A is the reservoir cross sectional area.

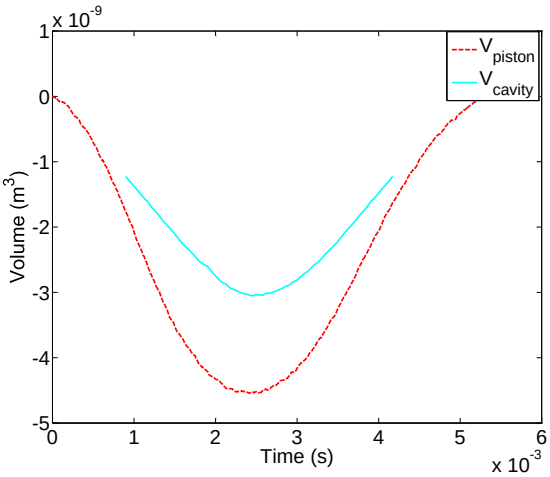

Fig. 6 Comparison between (V_{piston}) and (V_{cavity})

Influence of initial shape of the meniscus

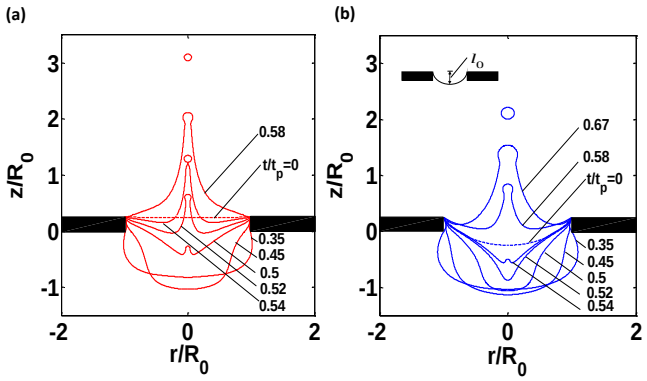

Fig. 7 Jetting simulation of silicone oil 10 cSt from 2 mm diameter nozzle with a fixed piston velocity amplitude 1.97 mm/s to show the influence of the initial meniscus form. (a) plane meniscus and (b) concave meniscus.

Experiments revealed that the initial shape of the unperturbed meniscus also played a role during the jetting process and the droplet size in an more pronounced way than in bubble bursting[38] . This was confirmed by numerical simulations, as shown in Fig. 7, where the evolution of the liquid interface is plotted for both a flat and a concave initial menisci. Simulations demonstrate that a concave meniscus with an initial maximum vertical distance of $l_0 = 0.5$ mm (i.e., $l_o/R_o = 0.5$, see Fig. 7(b)) increased the droplet size by 70% compared to the droplet produced by an initially flat meniscus. To further reduce the parametrical complexity of this study, the meniscus profile in the simulations will mimic those observed in the experiments.

The break up dynamics is complex and the correctness of numerical simulations are usually tested against well-known scaling laws of pinch off[43–47]. Figure 8 shows, from simulations, the diameter of the minimum jet's neck as a function of time for a 5 cSt jetting event. This shows the inviscid[45] regime and some indication of a transition towards the universal Inertial-Viscous

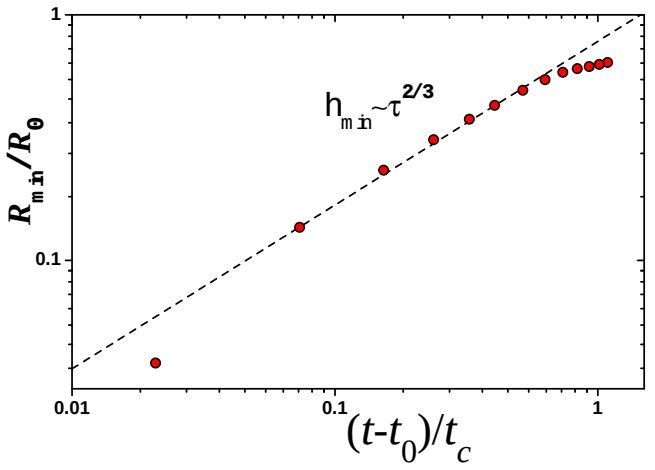

Fig. 8 Dimensionless neck radius as a function of dimensionless time to breakup for the case producing a droplet of $d = 800$ μ m.

regime[43,46]. The axes have been made dimensionless using the nozzle radius, $R_0 = 2$mm and capillary time $t_c = \sqrt{\rho R_0/\gamma}$.

4 Experimental and Numerical Results

Our studies were focused on determining which characteristics of the system and liquid properties where relevant to the jetting and droplet breakup. Experiments were carried out using silicone oils with viscosities of 5 and 10 cSt as the working fluids; these are well-characterised Newtonian liquids with negligible dependance on the ambient temperature or humidity. The physical properties of these liquids are listed in Table 1. The largest liquid cavity formed in our experiments was of 6 mm^3 and we found that the cavity size is directly proportional to the piston velocity. Fig. 1(a) shows the jetting process using silicone oil (10 cSt).

Table 1 Physical properties of the liquids used in the experiments.

Liquid	ρ (kg/m^3)	μ (cSt)	γ (mN/m)
Silicone oil(5 cSt)	912	5	21.9
Silicone oil(10 cSt)	936	10	23.1

Experimental results show that the size of the droplet is determined by a plethora of parameters, including the piston velocity amplitude v^- and the pulse width t_p, as seen in Fig. 1(b). Increasing the piston velocity causes a larger kinetic energy transfer to the fluid around the nozzle. As a consequence, a thinner jet and a smaller droplet are produced. In fact, the jet speed increases with a faster collapse (shorter pulse). The kinetic energy introduced not only affects the droplet size and its speed, but also determines the liquid ejection mode (single or multiple droplets). In particular, our interest are focused on the situation where a single droplet is ejected, as this is what most applications require, such as in inkjet. In addition to v^- and t_p, other important parameters are the liquid properties (viscosity μ, density ρ and surface tension σ), and the nozzle geometry (orifice's radius R_0 and thickness h).

The cases explored in the simulations are shown in Table 2. Figure 9 shows the numerical simulation of the jetting process of silicone oil (10 cSt) at a velocity amplitude v^- of 2 mm/s and pulse width of 4 ms. These numerical results along with the experiments provided sufficient evidence that allow us to propose a universal scaling argument, which is used to ultimately describe the dynamics across the explored parametric space.

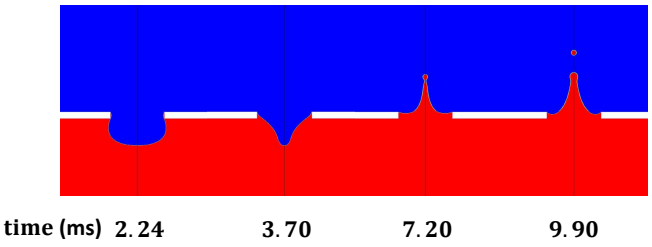

Fig. 9 Simulation of jetting out of cavity collapse from nozzle of 1 mm in radii.

In the range explored in this work (please see Table 2), we found that diminutive droplets are produced for low surface tensions: a single droplet of silicon oil (5 cSt) with a radius of 27 μm can be produced when the surface tension equals $\sigma = 21.9$ mN/m. The droplet size obtained from experiments and simulations, and their comparison are presented in Fig. 10. These results show that, under the conditions used in this work, numerical simulations are able to appropriately capture the experimental findings.

5 Scaling Arguments

Studies on bubble bursting[24–26,36,37] have identified a singularity involving the axial collapse of a wave front caused by the burst of the bubble film. The Ohnesorge number Oh$= \mu/(\rho\sigma R_o)^{1/2}$ governs the phenomenon, where R_o is the equivalent radius of the parent bubble in these studies. That collapse is physically similar to the one observed in the controlled cavity collapse here reported. The origin of the singularity can be found in the competition between the capillary speed and the viscous damping as the wave front advances in the meridional direction when we increase piston velocity. When the wave reaches the axis, the radi-

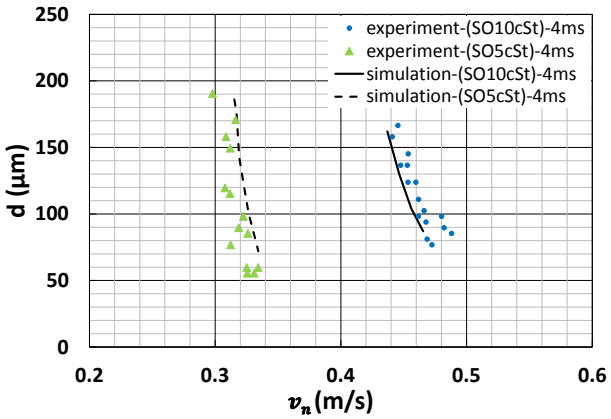

Fig. 10 Comparison between the droplet size in the numerical simulation and the experiments.

Table 2 Cases considered in the numerical simulation

Case	R_0 (mm)	h (mm)	l_0 (mm)	t_p (ms)	ρ (kg/m^3)	μ (cSt)	γ (mN/m)
A	0.5	0.25	0.38	4.2	936	10.0	23.1
B	0.75	0.25	0.38	4.2	936	10.0	23.1
C	1.0	0.5	0.38	4.2	936	10.0	23.1
D	1.0	0.75	0.38	4.2	936	10.0	23.1
E	1.0	0.25	0.38	3.0→4.2	936	1.0	23.1
F	1.0	0.25	0.38	4.2→5.0	936	2.0	23.1
G	1.0	0.25	0.38	4.2	912	5.0	21.9
H	1.0	0.25	0.38	4.2	936	6.0	23.1
I	1.0	0.25	0.38	4.2	936	7.5	23.1
J	1.0	0.25	0.38	4.2→6.0	936	10.0	23.1
K	1.0	0.25	0.38	4.2→5.0	936	10.0	60.0
L	1.0	0.25	0.38	4.2	1300	10.0	23.1
M	1.0	0.25	0.38	4.2	1800	10.0	23.1
N	1.0	0.25	0→0.5	4.2	936	10.0	23.1

ally collapsing momentum shoots the liquid ligament and ejects a droplet (i.e., creating net surface). In that instant, the local competition among the surface tension forces, inertia and viscous forces at the point of surface curvature reversal[38] leads to a scaling law where viscosity plays a counterintuitive role, producing a decrease in the size of the ejected ligament. This fact has been loosely interpreted as a *focusing* effect of viscosity[37] that produces very small droplets from bubble bursting. This can be understood in terms of the amount of initially available mechanical energy that viscosity dissipates just before the wave collapses at the axis: within a certain parametrical window, viscosity reduces the momentum of that wave, which consequently yields a smaller size scale of the ejection, but not necessarily a smaller scale of the velocity of ejection[38]. Therefore, there should be a limiting value of the viscosity above which no sufficient momentum is available at collapse to produce the ejection of a droplet. The existence of a critical Ohnesorge number $\mathrm{Oh}^* \simeq 0.04$[36], above which no droplets are ejected, supported this view. Experimental and simulations indicate that there is a minimum jet velocity in which a droplet breaks up and separates from the jet. Below this value, the kinetic energy is not high enough to overcome surface tension - the energy is enough to form a jet but it is then pulled back into the reservoir without breaking up. Any excess of kinetic energy above this limit forms a droplet. In summary, an excess of energy drives the jet velocity in all cases of cavity collapse, and controls the subsequent droplet ejection. In fact, in other phenomena, this energy surplus may come from several sources, e.g. film's surface energy in bubble bursting[24], the surface electrical charge in the onset of electrospray[31–35], or the kinetic energy in drops impacting a liquid pool[28]. In our system, this energy is introduced by the piston.

The analysis of the flow singularity at the collapse point can be made in terms of the local scales (geometrical and velocity scales) arising when the curvature of the surface at the axis undergoes a sudden change (the instants of curvature reversal). First, the amplitude and velocity of the wave that reaches the axis set a characteristic length L normal to the surface (i.e. in the axial direction) and a velocity scale V' in the radial direction, respectively (see Figure 11). Second, the size of the initiated jet front and its shooting speed set the droplet size d (i.e. the characteristic radial scale of the emission) and the scale of the axial velocity V_j, respectively. Using these four scales and the conservation equations of mass and momentum, Gañán-Calvo[38] obtained the scaling relations of d, L, and V' as functions of V_j that holds for this problem as well. The balance of all components of the momentum equation $\rho\left(\mathbf{v}_t + \mathbf{v}\cdot\nabla\mathbf{v}\right) + \sigma\nabla(\nabla_s\cdot\mathbf{n}) - \mu\nabla^2\mathbf{v} \simeq 0$ in the radial direction, assuming $O\left(\mathbf{v}_t\right) \sim O\left(\mathbf{v}\cdot\nabla\mathbf{v}\right)$, leads to:

$$\rho\frac{V_j^2}{L} \sim \mu\frac{V'}{L^2} \sim \frac{\sigma}{d^2}. \tag{3}$$

A third condition comes from mass continuity:

$$V'Ld \sim V_j d^2 \Longrightarrow V_j/V' \sim L/d. \tag{4}$$

These three conditions lead to:

$$d/l_\mu \sim \left(V_j/V_\mu\right)^{-5/3}, \tag{5}$$

$$L/l_\mu \sim \left(V_j/V_\mu\right)^{-4/3}, \tag{6}$$

$$V'/V_\mu \sim \left(V_j/V_\mu\right)^{2/3}, \tag{7}$$

where $l_\mu = \mu^2/(\rho\sigma)$ and $V_\mu = \sigma/\mu$ are the capillary-viscous length and velocity, respectively[38]. This scaling highlights the dependence of the ejected droplet size with the initial (or maximum) jet speed V_j. The results of this universal scaling are shown for both bubble bursting and the present system in Fig. 12, which

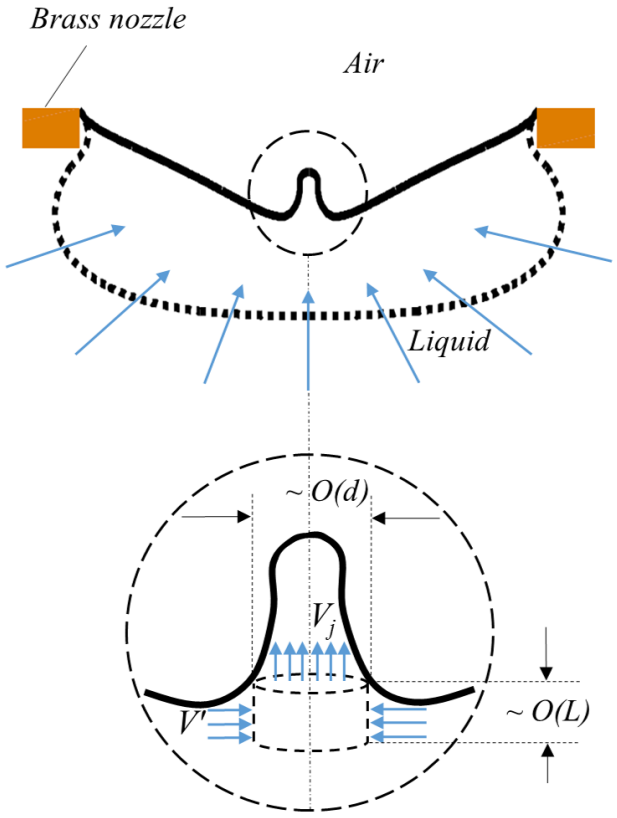

Fig. 11 Sketch of local spatial and velocity scales at the onset of jet ejection (surface curvature reversal at the axis).

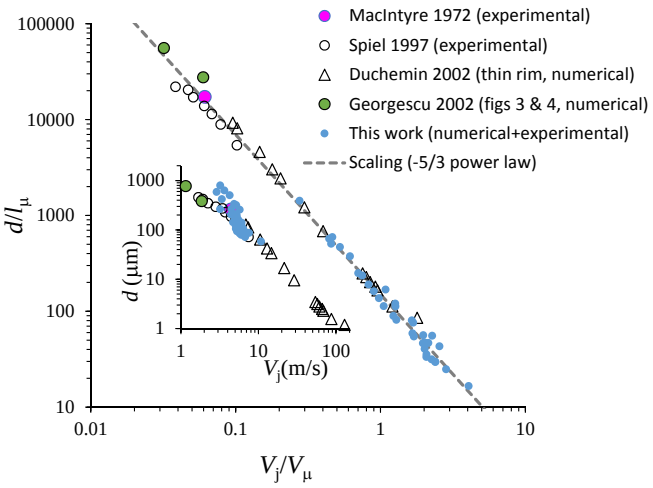

Fig. 12 Plots of the ejected droplet diameter dimensional vs. the maximum ejection speed for both numerical and physical experiments of bubble bursting and in the present system. Main plot: non dimensional values. Inset: dimensional values (d in μm, V_j in m/s).

shows that $d/l_\mu = A_d \left(V_j/V_\mu\right)^{-5/3}$, with $A_d \simeq 150$.

In practical applications, the scaling in Eq. 5 does not provide the general scaling of d as a function of the operation parameters as V_j is unknown. While simple energy considerations permits the calculation of this scaling for V_j in bubble bursting[38], the argument for cavity collapse and its additional degrees of freedom demand further considerations.

According to our experiments and simulations, the dynamics of droplet jetting from cavity collapse is determined by a set of nine dimensional parameters $\{\rho,\sigma,\mu,R_o,t_p,v_n,h,l_o,g\}$, where l_o is the initial meniscus deformation from a flat surface (seen in Fig. 7), g is the acceleration of gravity, and $v_n = v^- \left(\frac{D}{2R_o}\right)^2$. According to the Buckingham-Pi method, these can be reduced to 6 non-dimensional parameters as: $\{\mathrm{Oh}, t_p/t_c, v_n/v_c, l_o/R_o, h/R_o, \mathrm{Bo}\}$, where $t_c = \left(\rho R_o^3/\sigma\right)^{1/2}$, and $v_c = (\sigma/(\rho R_o))^{1/2}$ are the capillary time and velocity. Gravity effects[36] are considered negligible in our experiments, i.e $\mathrm{Bo} = \rho g R_0^2/\sigma \ll 1$, which effectively reduces the number of dimensionless parameters to five.

As previously discussed, a critical velocity v_{critical} defines the energy required to form a jet, but that is just short of producing a droplet. Under this notation, the effective mechanical energy excess $\varepsilon \simeq \Delta\left(\rho v_n^2/2\right) \simeq \rho v_n \Delta v$ should be proportional to $\Delta v = v_n - v_{\mathrm{critical}}$ assuming that $\Delta v \ll v_n$. In fact, we found that $\Delta v/v_n$ is below 0.20 for all the conditions producing droplets in our experiments. Consequently, Δv is used here as the convenient parameter that reflects the energy excess that should be fundamentally determined by the capillary velocity $v_c = (\sigma/(\rho R_o))^{1/2}$. Thus, the dependency of v_{critical} on the set of seven parameters $\{\rho,\sigma,\mu,R_o,t_{pw},l_o,h\}$ can be reduced to $v_{\mathrm{critical}}/v_c = f(\mathrm{Oh},\tau,\lambda_1,\lambda_2)$, where $\tau = t_{pw}/t_c$, $\lambda_1 = l_o/R_o$, and $\lambda_2 = h/R_o$.

Following the rationale found in a previous work[38], the conditions under which v_{critical} is met should correspond to that in which the total energy critically balances the kinetic energy of the ejected liquid column and the viscous dissipation. Thus, we introduce a critical Oh^* controlling the droplet generation above which no droplet ejection occurs. Given the number of operational parameters of our system, Oh^* cannot show the simple form exhibited in the bubble bursting problem. Following a systematic exploration of functional dependencies, and inspired by the work on bubble bursting[36,38] where a critical Ohnesorge number was also used, we propose the following relationship:

$$\frac{v_{\mathrm{critical}}}{v_c} = \frac{v_n - \Delta_v}{v_c} = k_0 \left[\left(\frac{\hat{\mathrm{Oh}}^*}{\hat{\mathrm{Oh}}} - 1\right) f(\mathrm{Oh},\tau,\lambda_1,\lambda_2)\right]^\alpha, \qquad (8)$$

where $\hat{\mathrm{Oh}} = \mu/(\sigma\rho\hat{R}_o)^{1/2}$ is defined for simplification. Here, $\hat{R}$ is a characteristic length of the system that should depend on the rest of parameters, $\{\tau,\lambda_1,\lambda_2\}$. A mathematical exploration of the simplest (polynomial) functional dependencies results in the following definitions:

$$\hat{R}_o = R_o \left(\lambda_1 + 5\lambda_2 + 2\lambda_2^2\right)^2 \left(\tau^2 + 0.05\tau + 0.06\right)^{-2}, \qquad (9)$$

and

$$f(\mathrm{Oh},\tau,\lambda_1,\lambda_2) =$$

$$\exp\left[(4.20\tau+1.47-44.10/\tau)\,\mathrm{Oh}+\lambda_1-2\lambda_2-\lambda_2^2\right]. \quad (10)$$

The numerical coefficients of Eqns. 9 and 10 were obtained using the experimental and simulation data, which yield a Pearson regression coefficient of $R^2 > 0.93$ for $\alpha = -0.093$ and a critical value of $\hat{\mathrm{Oh}}^* = 0.041$. This value is consistent with $\mathrm{Oh}^* \simeq 0.040$ obtained for bubble bursting[36,38] (assuming $\hat{R}_o$ as the equivalent parent bubble radius).

Finally, an analysis of the dominant parametrical dependence of V_j on the rest of parameters indicates that $V_j t_p/R_o \approx 1$. Again, among the infinite possible functional relationships, we propose an exponential form as:

$$V_j = A_o \frac{R_o}{t_p}\exp\left[k(\varphi)\right] \quad (11)$$

where $\varphi = \phi^{\beta}\Psi_1 + \Psi_2$, β, A_o and k are fitting parameters, with $\phi = \Delta v \rho R_o^2/(t_p\sigma)$ representing the last non-dimensional parameter to produce a rational expression for the role of the energy excess, and

$$\Psi_{1,2} = \Psi_{1,2}(\mathrm{Oh},\tau,\lambda_1,\lambda_2). \quad (12)$$

Our guide here is getting maximum data collapse using the simplest possible functional dependencies. Linear programming optimisation yields $\beta = 0.33 \pm 0.01$, $A_o = 20.2$, and $k = 0.8$, with

$$\Psi_1 = 1+0.8\mathrm{Oh}+5\mathrm{Oh}^2-350\mathrm{Oh}^3+0.12\tau+0.055/\tau+0.25\lambda_1+$$
$$+0.07\lambda_1^2+0.7\lambda_2-0.15\lambda_2^2 \quad (13)$$

and

$$\Psi_2 = -0.2\mathrm{Oh}-3\mathrm{Oh}^2+0.025/\tau-0.06\lambda_1+0.09\lambda_1^2-2.4\lambda_2. \quad (14)$$

In summary, we have six fitting parameters $\{\mathrm{Oh}^*, A_d, A_o, \alpha, \beta, k\}$ and four polynomic adjustable functional forms (9), (10), (13) and (14).

Experiments and simulations were performed in the range of $3 < Re < 60$ and the predicted speed. These are shown in Fig. 13. As discussed, droplet speed and droplet size are connected through the scaling argument presented in Eq. 5; i.e. a potential law with a $-5/3$ exponent. By applying this scaling to Eq. 11, one can obtain the droplet size as shown in Fig. 14. These jetting parameters covers the known range in which single pinch-off droplets are known to exist[48].

6 Conclusions

In this work we have presented experimental and numerical results aimed at gaining a better understanding of a novel method to produce droplets significantly smaller than the nozzles from which they emerge. Moreover, we have proposed a physical model and scaling law to predict the size of the generated droplet based on the liquid properties, the nozzle geometry, and the driving waveform. The resulting system can operate on a drop-on-demand mode, where the droplet generation is controlled by the piston velocity and the pulse width. This approach would also greatly benefit, for instance, grey-scale printing applications.

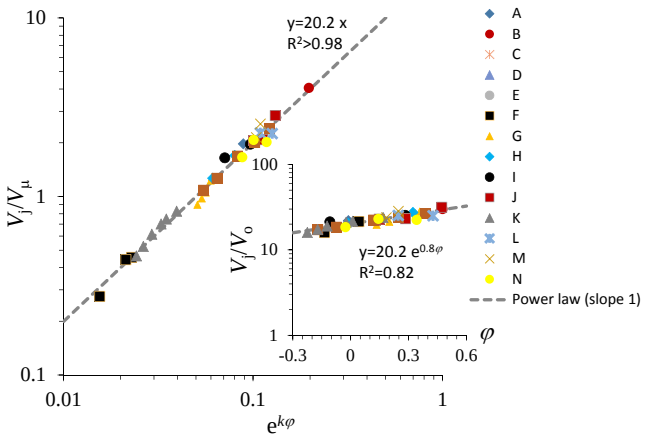

Fig. 13 Jet velocity V_j made dimensionless with either $V_o = R_o/t_p$ (inset) or V_μ, showing the agreement of the scaling proposed. The open symbols represent experimental data, while the closed symbols represent numerical data.

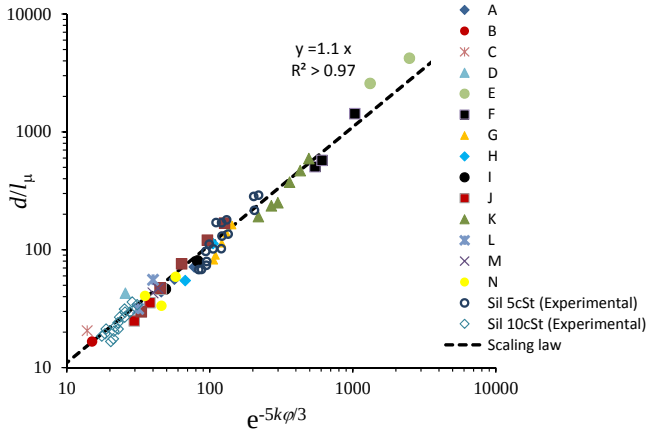

Fig. 14 Dimensionless droplet size $\frac{d}{l_\mu}$ as a function of the scaling variable $\exp(-5k\varphi/3)$.

Acknowledgements

This work was supported by the Royal Society (UF120319, URF\R\180016, and RGF\EA\180061), the John Fell Oxford University Press Research Fund (0005176), the EPSRC -UK (EP/P024173/1), and the Ministerio de Economía y Competitividad, Plan Estatal 2013-2016 Retos, project DPI2013-46485-C3-1-R.

References

1 Doring, M. Ink-jet Printing *Philips Tech. Rev.* **1982** 40, 192-198.

2 Ridley, B. A.; Nivi, B.; Jacobson, J. M. All-Inorganic Field Ef-

fect Transistors Fabricated by Printing *Science* **1999** 286, 746-749.

3 Schena, M.; Heller, R. A; Theriault, T. P.; Konrad, K.; Lachenmeier, E.; Davis, R. W. Microarrays: biotechnology's discovery platform for functional genomics *Trends Biotechnol* **1998** 16, 301-6.

4 Graham, A. D.; Olof, S.N.; Burke, M. J.; Armstrong, J. P. K.; Mikhailova E. A.; Nicholson J. G.; Box S. J.; Szele F. G. , Perriman A. W. and Bayley H. High-Resolution Patterned Cellular Constructs by Droplet-Based 3D Printing *Scientific Reports* **2017** 7, 7004

5 Guo Y., Patanwala, H.S.; Bognet,B.; Ma, A. W. K. Inkjet and inkjet-based 3D printing: connecting fluid properties and printing performance *Rapid Prototyping Journal* **2002** 33, 562-576

6 Murr, L. E.; Johnson W. L. 3D metal droplet printing development and advanced materials additive manufacturing *J. Mat. Res. and Tech.* **2017** 6, 77-89.

7 Basaran, O.A. Small-Scale Free Surface Flows with Breakup: Drop Formation and Emerging Applications, *AIChE Journal* **2002**, 48, pp. 1842-1848.

8 Basaran, O.A.; Gao, H.; Bhat, P. P. Nonstandard Inkjets, *Annu. Rev. Fluid Mech.* **2013**, 45, pp. 85-113.

9 Castrejón-Pita, J. R.; Baxter, W. R. S.; Morgan, J.; Temple, S.; Martin, G. D.; Hutchings, I. M. Future, Opportunities and Challenges of Inkjet Technologies. *Atomization Spray* **2013** 23, 541.

10 Hoath, S.D. (Ed.) Fundamentals of Inkjet Printing: The Science of Inkjet and Droplets; *Wiley-VCH Verlag GmbH & Co.*: Weinheim, Germany, **2016**.

11 Zoltan, S. I. Pulsed droplet ejecting system U. S. Patent **1972** No. 3,683,212.

12 Kyser, E. L.; Sears, S. B. Method and Apparatus for Recording with Writing Fluids and Drop Projection Means Therefor **1976** U. S. Patent No. 3,946,398.

13 Montanero, J. M.; Gañán-Calvo, A. M.; Acero, A. J.; Vega, E. J. Micrometer glass nozzles for flow focusing *J. Micromech. Microeng.* **2010** 20, 075035.

14 Kimura, J.; Kawana, Y.; Kuriyama, T. An Immobilized Enzyme Membrane Fabrication Method Using an Ink Jet Nozzle *Biosensors* **1988** 4, 41-52.

15 Lloyd, W. J.; Taub, H. H. Ink jet printing *Output Hardcopy Devices* **1988** 13, 311-370.

16 Bernardini, G. L.; Rampy, B. A.; Howell, G. A.; Hayes, D. J.; Frederickson, C.J. Applications of piezoelectric fluid jetting devices to neuroscience research. *J. Neurosci. Methods* **1991** 38, 81-8.

17 Brennan, T. M. Method and apparatus for conducting an array of chemical reactions on a support surface U.S. Patent **1995** No. 5,474,796.

18 Le, H. P. Progress and Trends in Ink-jet Printing Technology *J. Imaging Sci. Technol* **1998** 42, 49-62.

19 Perçin, G.; Atalar, A.; Degertekin, F. L.; Khuri-Yakub, B. T. Micromachined two-dimensional array piezoelectrically actuated transducers *Appl. Phys* **1998** 72, 1397.

20 Chen, A. U.; Basaran, O. A. A new method for significantly reducing drop radius without reducing nozzle radius in drop-on-demand drop production *Phys. Fluids* **2002** 14, L1-L4.

21 Chen, A. U.; Basaran, O. Method and apparatus for producing drops using a drop-on-demand dispenser U.S. Patent **2003** No. 6,513,894

22 Xu, X.; Basaran, O. A. Method for producing ultra-small drops U.S. Patent **2012** No. 8,186,790.

23 Burr, R. F.; Tence, D. A.; Le, H. P.; Adams, R. L.; and Mutton, J. C. Method for producing ultra-small drops U.S. Patent **1996** No. 5,495,270.

24 MacIntyre, F. Flow Patterns in Breaking bubbles *J. Geophys. Res.* **1972** 77, 5211-5228.

25 Duchemin, L.; Popinet, S; Josserand, C.; Zaleski, S Jet formation in bubbles bursting at a free surface *Phys. Fluids* **2002** 14, 3000-3008.

26 Spiel, D. E. On the births of jet drops from bubbles bursting on water surfaces *J. Geophys. Res.* **1995** 100, 4995-5006.

27 Ghabache, E.; Liger-Belair, G.; Antkowiak, A.; Séon, T. Evaporation of droplets in a Champagne wine aerosol *Sci. Rep.* **2016** 6, 25-48.

28 Yarin, A. L. Drop impact dynamics: Splashing, spreading, receding, bouncing ... *Annu. Rev. Fluid Mech.* **2006** 38, 159-192.

29 Castrejón-Pita, A. A.; Castrejón-Pita, J. R.; Martin, G. D. A novel method to produce small droplets from large nozzles *Rev. Sci. Instrum.* **2012** 83, 115105.

30 Gañán-Calvo, A. M. Generation of Steady Liquid Microthreads and Micron-Sized Monodisperse Sprays in Gas Streams *Phys. Rev. Lett.* **1998** 80, 285.

31 Collins, R. T.; Harris, M. T.; Basaran, O. A. Breakup of electrified jets. *J. Fluid Mech.* **2007** 588, 75-129.

32 Higuera, F. J. Flow rate and electric current emitted by a Taylor cone. *J. Fluid Mech.* **2003** 484, 303-327.

33 Collins, R. T.; Sambath, K.; Harris, M. T.; Basaran, O. A. Universal scaling laws for the disintegration of electrified drops. *Procc. Nat. Acad. Sci.*. **2013** 110, 4905-4910.

34 Higuera, F. J.; Ibáñez, S.E.; Hijano, A.J.; Loscertales, I. G.; Pulsating emission of droplets from an electrified meniscus. *J. Aerosol Science*. **2013** 66, 193-208.

35 Gañán-Calvo, A. M.; López-Herrera, J. M.; Rebollo-Muñoz, N.; Montanero, J. M. The onset of electrospray: the universal scaling laws of the first ejection *Sci. Rep.* **2016** 6, 32357-9.

36 Walls, P. L. L.; Henaux, L.; Bird, J. C. Jet drops from bursting bubbles: How gravity and viscosity couple to inhibit droplet production *Phys. Rev. E* **2015** 92, 021002(R).

37 Ghabache, E.; Séon, T. Size of the top jet drop produced by bubble bursting *Phys. Rev. Fluids* **2016** 1, 051901(R).

38 Gañán-Calvo, A. M. Revision of Bubble Bursting: Universal Scaling Laws of Top Jet Drop Size and Speed *Phys. Rev. Lett.* **2017** 119, 204502-4.

39 Deike, L.; Ghabache, E.; Liger-Belair, G.; Das, A. K.; Zaleski, S.; Popinet, S.; Séon, T. Dynamics of jet produced by bursting bubbles *Phys. Rev. Fluids* **2018** 3, 013603.

40 Dataset for the graphs in Figure 3 are available as supplemental material.

41 Issa, R. I. Solution of the implicitly discretised fluid flow equations by operator-splitting *J. Comput. Phys.* **1986** 62, 40-65.

42 Leer, B. V. Towards the ultimate conservative difference scheme. V - A second-order sequel to Godunov's method *J. Comput. Phys.* **1979** 32, 101-136.

43 Eggers, J. Universal Pinching of 3D Axisymmetric Free-Surface Flow. *Phys. Rev. Lett.* **1993** 71, 3458

44 Eggers, J. Theory of drop formation. *Phys. Fluids* **1995** 7, 941

45 Day, R. F.; Hinch, E. J.; and Lister, J. R. Self-similar capillary pinchoff of an inviscid fluid. *Phys. Rev. Lett.* **1998** 80, 704.

46 Chen,A. U.; Notz, P. K.; and Basaran, O. A. Computational and experimental analysis of pinch-off and scaling. *Phys. Rev. Lett.* **2002** 88, 174501.

47 Castrejón-Pita, J. R.; Castrejón-Pita, A. A.; Thete, S. S.; Sambath, K.; Hutchings, I. M.; Hinch, J.; Lister, J. R. ; Basaran, O. A. Plethora of transitions during breakup of liquid filaments. *Proc. Natl. Acad. Sci.* **2015** 112, 4582-4587.

48 Derby, B. Inkjet Printing of Functional and Structural Materials: Fluid Property Requirements, Feature Stability, and Resolution *Annu. Rev. Mat. Res.* **2010** 40, 395-414.